frontiers | Frontiers in Earth Science

TYPE Original Research
PUBLISHED 10 January 2023
DOI 10.3389/feart.2022.1047557

Check for updates

OPEN ACCESS

EDITED BY
Mingjun Zou,
North China University of Water Resources and Electric Power, China

REVIEWED BY
Taotao Cao,
Hunan University of Science and Technology, China
Teng Li,
Xi'an Shiyou University, China

*CORRESPONDENCE
Wei Jiang,
jiangwei3q@163.com

SPECIALTY SECTION
This article was submitted to Economic Geology,
a section of the journal
Frontiers in Earth Science

RECEIVED 18 September 2022
ACCEPTED 23 September 2022
PUBLISHED 10 January 2023

CITATION
Jiang W, Zhou Y, Wu C and Du M (2023), Fractal characteristics and theirs influence on methane adsorption in high-rank coals with NMR.
Front. Earth Sci. 10:1047557.
doi: 10.3389/feart.2022.1047557

Fractal characteristics and theirs influence on methane adsorption in high-rank coals with NMR

Wei Jiang[1,2,3]*, Ying Zhou[1,2], Caifang Wu[3] and Mingyang Du[1,2,3]

[1]School of Earth Sciences and Engineering, Suzhou University, Suzhou, China, [2]National Engineering Research Center of Coal Mine Water Hazard Controlling, Anhui, China, [3]School of Resource and Geoscience, China University of Mining and Technology, Xuzhou, China

To further understand the pore structure characteristics and their effect on CH_4 adsorption capacity for high-rank coals. Based on 11 fresh coal samples from the Zhina coalfield of South China. We analyzed the pore structure characteristics of coal samples by low-temperature liquid-nitrogen adsorption (LP-N_2A) measurements. On the basis of nuclear magnetic resonance (NMR), we obtained the fractal dimensions of different types of pores by the new model, studied the relationship between the fractal dimensions, and the characteristic parameters of coals (composition and pore characteristics) and discussed the influence of the fractal dimensions on CH_4 adsorption. The results show that according to LP-N_2A isotherms, all coals can be classified into three types. The micropores provide the largest proportion of the specific surface area (SSA) of coals. Two fractal dimensions, D_a (adsorption pore) and D_s (seepage pore), ranged from 2.471 to 2.805 and from 2.812 to 2.976, which were acquired in the saturated water condition by NMR. Furthermore, D_a and D_s have different correlations with ash yield, carbon contents, moisture, SSA and irreducible fluid porosity. The coal composition and pore parameters have much greater control over fractal dimensions. Moreover, the different fractal dimensions have different influences on methane adsorption. With the increase of D_a, the methane adsorption capacity is enhanced, but it is weakened with the increase of D_s. The high-rank coals have more SSA with higher D_a and provide more adsorption sites for CH_4. Langmuir pressure P_L has different correlations with fractal dimensions. D_a decreases with the increase of P_L. The adsorption velocity is faster with higher D_a. Thus, the fractal dimensions are the comprehensive reflection of differences among the physical properties of coal and are able to show the effect of coal properties on methane adsorption fully.

KEYWORDS

nuclear magnetic resonance, fractal dimension, coalbed methane, adsorption, coal pore structure

1 Introduction

Coal is a complex and heterogeneous porous medium. Its internal pore surface area is much larger than its external surface area which can be neglected. The pore surface with strong adsorption ability is the primary storage and migration of coalbed methane (CBM) (Alexeev, 1977; Meyers, 1982). The structure and developmental features of pores perform a significant control function in adsorption capacity, desorption capacity and permeability of coal reservoirs, which directly affects the exploration efficiency of CBM. Meanwhile, the unstable CBM production is influenced by the complex features of pore-fracture, buried depth of coal seam and geothermal dynamics (Johnson and Flores, 1998; Saboorian-Jooybari, 2016; Zhao et al., 2019). Thus, it is a great significance to characterize coal reservoirs by researching the storage capacity and migration mechanism of pores in coal reservoirs (Dullien, 1991).

At present, defining the coal pore system, there are various classifications of qualitative descriptions of pores in coal reservoirs (Hodot, 1966; Sing, 1982; Fu et al., 2005; Cai et al., 2013a). Based on gas adsorption–desorption, Hodot's classification (Hodot, 1966) is widely used. The pores are divided into four types: micropores (less than 10 nm), transition pores (10–100 nm), mesopores (100–1000 nm) and macropores (more than 1,000 nm). Pores (less than 100 nm) are adsorption pores which play a crucial role in CBM adsorption and diffusion pores (Cai et al., 2013b). In the present study, the pore characteristics of coal reservoir are studied by many methods and technologies, such as mercury intrusion porosimetry (MIP) (Gao et al., 2018; Ju et al., 2018), scanning electron microscopy (SEM) (Shan et al., 2015; Li et al., 2020a), N_2 adsorption-desorption and CO_2 gas adsorption (Acevedo and Barriocanal, 2015; Li et al., 2019; Nie et al., 2020), atomic force microscope (AFM) (Pan et al., 2015), small-angle X-ray scattering (SAXS) (Ferro et al., 2012; Coetzee et al., 2015; Liu and He, 2017) and nuclear magnetic resonance (NMR) (Lee and Lee, 2013; Li et al., 2017). The result shows that the pore structure of coal has a fractal feature within a certain scale range (Fu et al., 2005; Shi et al., 2006; Yao et al., 2009; Liu et al., 2015; Peng et al., 2017). However, these technical methods may cause the decrease of pore diameter, the damage of coal matrix system and the loss of some important details of coal reservoir (Yao and Liu, 2012). NMR is an efficient experimental method to study the pore properties of coal reservoirs. The NMR technique is widely applied in petrophysical features, shapes, sizes and porosity of pores, because of its rapid, accurate and high-resolution characteristics. NMR T_2 cutoff value (T_{2C}) is an important parameter for irreducible water saturation calculation, pore size distribution (PSD) and permeability prediction. Ge et al. (2014) studied the influential factors of T_{2C} and proposed the predicating model for T_{2C} value by multiple linear regressions of multifractal parameters. Yao et al. (2010) designed the NMR experiments of 100% water-saturated and irreducible water coal samples, respectively. Results show that the relaxation times corresponding to the adsorption-pore (< 100 nm), seepage-pore (> 100 nm) and fracture are 0.5–2.5 ms, 20–50 ms and >100 ms, respectively. Meanwhile, the NMR-based permeability model is built on the basis of the data of calculated irreducible and producible porosities. Zheng et al. (2020) divided T_2 cutoffs into two types: the absolute irreducible fluid T_2 cutoffs (T_{2C1}) and absolute movable fluid T_2 cutoff (T_{2C2}); Based on the dual T_2 cutoffs model, the pore fluid typing of coal is divided into three types: absolute irreducible fluid ($T_2 < T_{2C1}$), partial movable fluid ($T_{2C1} < T_2 < T_{2C2}$) and absolute movable fluid ($T_2 > T_{2C2}$).

Because of the complexity and anisotropy of the pore structure of the coal reservoir, it is difficult to give an accurate description by the traditional geometrical method and is unable to measure by fixed scale. The fractal theory is an effective method to quantitatively describe pore structure features (Song et al., 2013; Wang et al., 2013). Based on the isotherms of N_2 gas adsorption/desorption, adopting the fractal Frenkel–Halsey–Hill (FHH) method, the fractal dimensions D_1 and D_2, which represent the irregularity of pore surface and heterogeneity of pore structure, are obtained (Yao et al., 2008). Coupled with CH_4 isotherm adsorption experiments, D_1 has more significant influence than D_2 on adsorption capacity (Li et al., 2015). Song et al. (2017) analyzed the fractal characteristics of nanopores in tectonically deformed coals on the basis of mercury intrusion and N_2/CO_2 gas adsorption experiments. They found that the fractal dimension (<8 nm) has an important role in the adsorption capacity. Additionally, previous researchers have found that the NMR fractal theory is used to study the pore-fracture characteristics of coal (Li et al., 2013; Sun et al., 2015; Ouyang et al., 2016). Based on the NMR T_2 spectrum, the fractal dimensions are divided into D_1(adsorption pores) and D_2(seepage pores). D_2 has a significant influence on the permeability of the coal reservoir (Chen et al., 2018). Zhou et al. (2016) calculated the adsorption space fractal (D_{NMRA}), seepage space fractal (D_{NMRS}) and moveable fluid space fractal (D_{NMRM}) in low-rank coals, respectively. They demonstrated the model between permeability and D_{NMRM}. With MIP and NMR methods, MIP and NMR permeability were estimated by the modified Kozeny-Carman Equation and movable porosity-permeability model, respectively (Li et al., 2020b). Zhou et al. (2022) proposed a novel model by the low-field NMR and obtained the fractal dimensions of accessible, inaccessible and total pores, respectively. Nevertheless, the correlation between CH_4 adsorption capacity and NMR fractal dimensions of coals has not been sufficiently researched.

In this paper, we collect 11 coal samples from the Zhina coalfield of South China and carry out the experiment analyses to investigate the characteristics of pores and coal adsorption by the LP-N_2A, NMR and CH_4 isotherm adsorption methods. According to the experimental data and results analysis, we

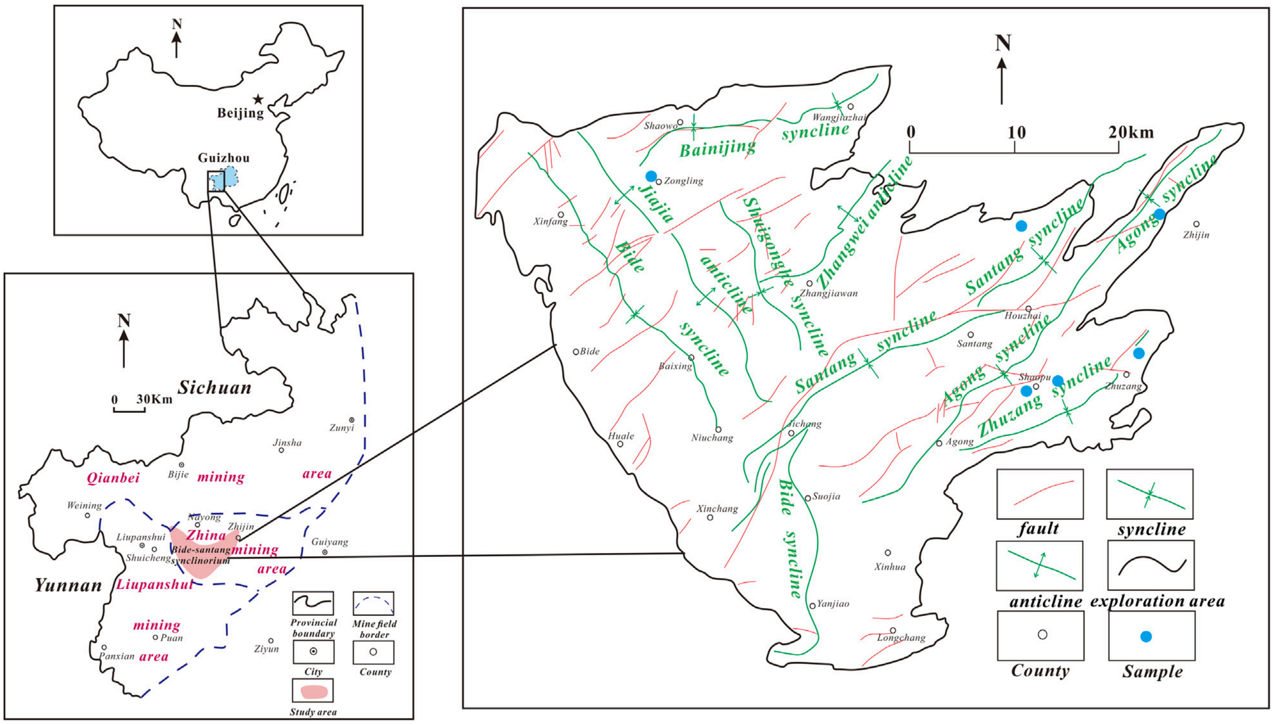

FIGURE 1
Location map showing the distribution of sampling points in the Bide-Santang Basin, China (modified from Yang et al., 2014, 2019).

analyze the pore characteristics of coal samples, calculate the fractal dimensions of different pore types, and study the relationships between CH_4 adsorption capacity and fractal dimensions.

2 Materials and methods

2.1 Sampling

Eleven samples were collected from the Bide-Santang Basin, which is a CBM reservoir of multiple coal seams in the Zhina coalfield, Guizhou Province (Figure 1). Zhina coalfield, located in western Guizhou Province, is the largest anthracite coal occurrence area in China. The coal-bearing strata of the Bide-Santang Basin are the Longtan and Changxing formations of Upper Permian, with a formation thickness of 300–450 m. In the upper Permian, the coal-bearing formation was mainly developed at continental, continental-marine transitional and shallow marine sedimentary facies. Multiple coal-bearing strata formed during this period due to frequent sea transgression and regression. Tectonic activities during the Yanshan and Himalayan formed large synclines and synclinoria, which became important structures controlling coal in the region (Yang et al., 2019). The gas content of coal seam of in Longtan Formation is generally high. The average gas content is 10–15.78 m^3/t. The reservoir pressure is 2.95–11.59 MPa. The *in-situ* permeability of coal reservoir is low, and its average value is 0.14 mD (Cheng et al., 2021). Table 1 shows the collected samples and their locations. All the samples whose size was 30 cm×30cm×30 cm were wrapped with plastic wrap according to the Chinese Standard (GB/T 19,222–2003) and quickly packed. The grind and screening of samples were completed in the laboratory after sampling. According to GB/T6948-2008 and GB/T212–2008, samples (less than 0.200 mm in particle diameter) were selected for proximate analysis and maximum vitrinite reflectance.

2.2 CH4 isotherm adsorption experiments

Experiments were performed at the China petroleum exploration and development research institute Langfang branch using TerraTek Isothermal Adsorption and Desorption Experimental System (IS–300), according to Chinese standard (GB/T 19,560–2008). The sensitivity of the temperature sensor and pressure sensor is 0.3 C and 0.001°MPa, respectively. All the

TABLE 1 Coal analysis results for samples.

Sample ID	Vitrinite reflectance ($R_{o,max}$ %)	Coal-bearing strata	Proximate analysis(%)[a]			
			M_{ad}	V_{daf}	A_{ad}	FC_{ad}
X-1	2.30	longtan formation	0.52	12.0	25.16	62.81
X-2	3.21	longtan formation	1.66	6.70	7.83	88.65
X-3	3.32	longtan formation	1.25	5.48	13.68	85.28
X-4	3.02	longtan formation	1.08	6.95	11.15	81.03
X-5	3.40	longtan formation	1.55	6.21	14.56	82.56
Y-1	2.60	changxing formation	0.42	11.17	15.07	72.8
Y-2	2.74	longtan formation	1.14	11.37	18.76	70.48
Y-3	2.90	longtan formation	0.68	7.56	16.87	79.52
Y-4	2.70	longtan formation	0.70	8.82	12.16	77.36
Y-5	3.11	longtan formation	0.83	7.50	11.87	79.86
Y-6	2.86	longtan formation	0.94	8.08	9.95	80.82

Note: The approximate content of fixed carbon (FC_{ad}), ash (A_{ad}) and moisture (M) are from the air-dried basis of samples; V_{daf} is volatile matter content from the dry ash-free basis of samples.

coal samples were broken, smashed and screened to a size range of 0.18–0.25 mm. Then, the moisture-equilibrium treatment of 200 g samples was carried out. The screened experimental samples were put in an incubator with oversaturated K_2SO_4 solution. The samples were weighed every other 24 h until the quality change was below 2 percent of their weight. The experimental temperature was 30°C, and the experimental pressure range was 0–13 MPa. The time of adsorption equilibrium kept above 12 h.

2.3 LP-N_2A and NMR measurement

LPN_2A was performed for the 11 coal samples using a Micromeritics ASAP 2000 surface area measurement. First, the coal samples were ground into a size range of 0.25–0.40 mm. Approximately 5 g of coal particles was placed in a vacuum oven and degassed at 105 C for 12 h to remove air, free moisture and other impurities. Then, degassed samples were exposed to N_2 with purity greater than 99.99% at a temperature of 77.3°K. The range of relative pressure (P/P_0) was from 0.01 to 0.995. Moreover, the Brunauer–Emmett–Teller (BET), Barrett–Joyner–Halenda (BJH) and density functional theory (DFT) models were applied to evaluate the specific surface area (SSA), pore volume (PV) and PSD, respectively (Brunauer et al., 1938; Barrett et al., 1951; Geerlings et al., 2003).

NMR measurement was performed at SGS Unconventional Petroleum Technical Testing Limited Company, following specifications of surveys SY/T 6490-2007. Firstly, several horizontal cylindrical core plugs with a diameter of 2.5 cm were drilled; Secondly, all core plugs were placed in a drying oven until drying to constant weight, then saturated with 100% saturated standard brine for 24 h; Thirdly, core plugs were placed in the probe of low magnetic field resonance core analyzer to test the transverse relaxation time T_2 and worked out relaxation time spectrum of T_2 by inversion. Finally, core plugs were placed in a centrifuge to dehydrate, and the centrifugal pressure was 200°psia.

2.4 Fractal theory based on NMR

Lots of papers have extensively reported the fractal dimensions of NMR (Zhang et al., 2007; Wang et al., 2011; Zhang and Weller, 2014). The fractal dimensions of NMR are obtained from the NMR data of the irreducible water and saturated water by establishing the equation of fractal dimension of coal pores (Ouyang et al., 2016; Zhou et al., 2018), But the low correlation coefficient of fractal makes these methods unsuitable for obtaining quantitative heterogeneity for porous media. We calculated the fractal dimension of pores by the new model (Zhou et al., 2022).

The critical characteristic of fractal targets in nature is self-affinity of dimension and can be quantified by a power-law function (Lai et al., 2018).

$$N(r) \propto r^{-D} \tag{1}$$

Where r is the pore size for rock, D is the fractal dimension, $N(r)$ is the number of objects whose sizes are greater than the size.

The pore size distribution could be directly related to the distribution of NMR T_2 relaxation time (Daigle and Johnson, 2016). The formula can be expressed as

$$\frac{1}{T_2} = F_s \frac{\rho}{r} \tag{2}$$

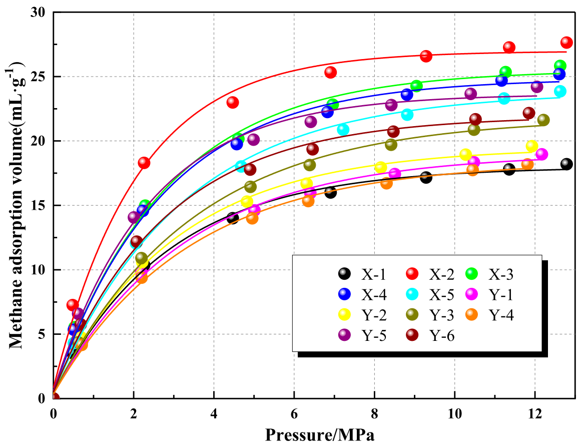

FIGURE 2
Results of methane adsorption test and the fitting Langmuir curves.

If the coal structure is a tube, then Fs = 2; Fs = 3 for spherical; ρ is the strength of transverse relaxation;

The signal amplitude at the T_{2i} relaxation time is a function of the number of protons, corresponding to the pore volume of pore radius r_i (Dillinger and Esteban, 2014). The total PV (V_p , %) represents the sum of the signal amplitudes from minimum to maximum T_2 values, then V_p can be expressed as

$$V_p = \sum_{i=1}^{n} V_{pi} \tag{3}$$

Where V_{p1} and V_{pn} are the signal amplitude at the minimum and maximum T_2 value, respectively. V_{pi} corresponds to the signal amplitude at T_{2i} value.

The pore morphology of coal samples is assumed to be spherical, then the number of pores with a specified size r_i can be given by

$$N_i = \frac{V_{pi}}{\frac{4}{3}\pi r_i^3} = \frac{V_{pi}}{36\pi\left(\rho T_{2i}\right)^3} \tag{4}$$

Therefore, the number of pores whose pore size is larger than r_i is expressed as

$$N(r) = \sum_{j}^{n} N_i = \sum_{j}^{n} \frac{V_{pi}}{\frac{4}{3}\pi r_i^3} \tag{5}$$

Where $j = i + 1$

By combining Equations 1, 2, and 5:

$$N(r) = \frac{V_{pi}}{36\pi\left(\rho T_{2i}\right)^3} \propto \left(3\rho T_{2i}\right)^{-D} \tag{6}$$

Using logarithms for Eq. 6, is revised as

$$\log\left(\sum_{j}^{n} \frac{V_{pi}}{(T_{2i})}\right) + \log\frac{1}{A} = -D\log B - D\log(T_{2i}) \tag{7}$$

Where $A = 36\pi\rho^3$ and $= 3\rho$. $-DlogB$ and $log(1/A)$ are the constants. The fractal dimension can be obtained by the slope of the optimal fit line in the log–log plot of pore number $N(r)$ against pore radius (T_2) .

3 Results

3.1 Coal rank, coal component and CH_4 adsorption analysis results

As seen from Table 1, the maximum vitrinite reflectance of coals ranges from 2.30 to 3.40%, which belongs to high-rank coal. Moisture contents of coals increase from 0.52 to 1.66%, ash yields of coals increase from 7.83 to 25.16%, carbon contents of coals reduce from 88.65 to 62.81% and volatile matter contents of most samples increase from 5.48 to 12.00%. The composition of coal samples is complicated, and each component concentration has the noticeable differences. Most of the coal samples are

TABLE 2 Fitting results of methane adsorption test.

Sample ID	Langmuir volume (m^3/t)	Langmuir pressure (MPa)	Equilibrium moisture (wt%)	Correlation coefficients R^2
X-1	21.65	2.45	4.58	0.9972
X-2	31.04	1.57	6.05	0.9695
X-3	30.76	2.42	5.37	0.9973
X-4	29.86	2.34	5.45	0.9975
X-5	29.48	2.98	4.86	0.9976
Y-1	23.82	3.14	5.07	0.9972
Y-2	24.17	2.82	4.25	0.9971
Y-3	27.56	3.34	6.03	0.9980
Y-4	23.24	3.26	3.60	0.9977
Y-5	28.27	2.03	4.80	0.9955
Y-6	26.83	2.50	2.99	0.9966

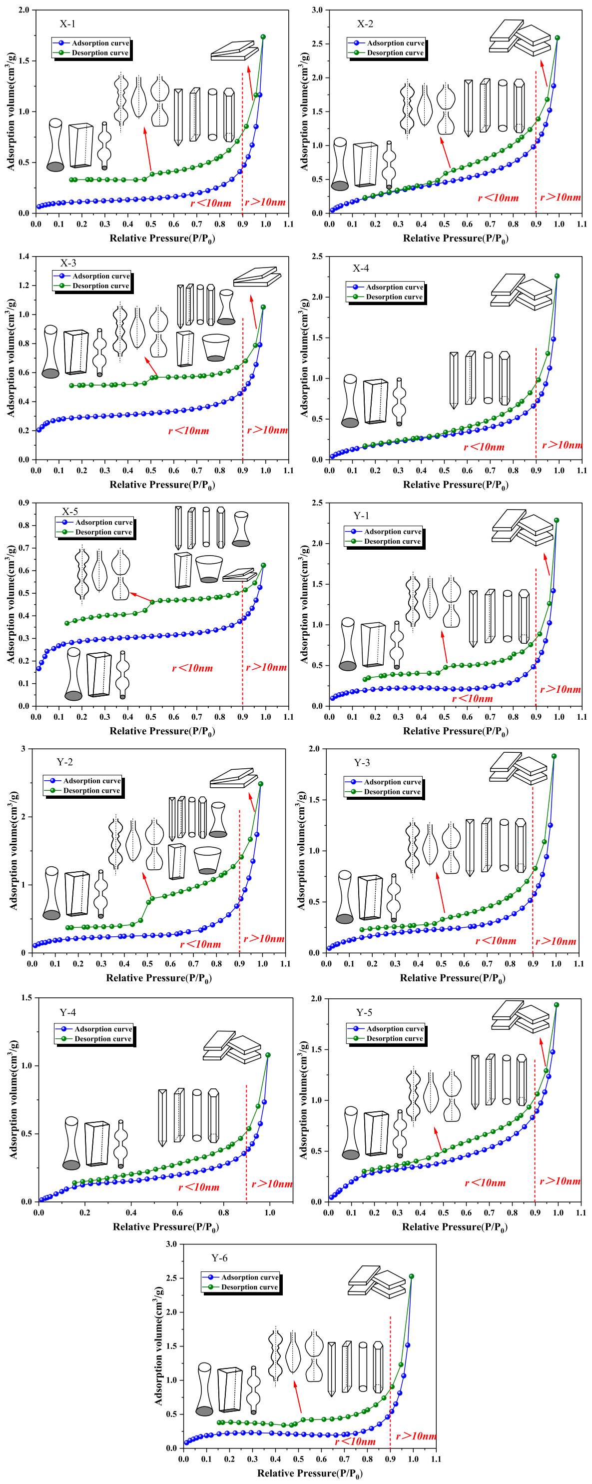

FIGURE 3
N_2 adsorption/desorption isotherms of all the samples.

low–middle ash coal. Vitrinite is the dominant maceral composition for all coal samples.

The results of the methane adsorption experiment of each coal sample are shown in Figure 2. The experimental results are fitted by the Langmuir equation:

$$V = \frac{V_L * P}{(P_L + P)} \tag{8}$$

Where P is the pressure, MPa; V is the absorption at the pressure P, m^3/t; V_L is the Langmuir volume, m^3/t; P_L is the Langmuir pressure, MPa.

The fitted results are shown in Table 2. The degree of the fitting is high by the Langmuir equation about the methane adsorption curves of all coal samples. The Langmuir volume ranges from 21.65 ml/g to 31.04 ml/g, and the Langmuir pressure ranges from 1.57°MPa to 3.34 MPa. It shows that the adsorption capacity of different coal samples has the certain difference. But methane adsorption of coal samples has a different growth rate with increasing pressure. Methane adsorption of some coal samples increases rapidly at low pressure but flattens at high pressure. Yet methane adsorption of some other coal samples increases slowly (Li et al., 2013). For example, the methane adsorption of coal sample X-2 is about 17.4 ml/g at 2 MPa pressure, but that of coal sample X-3 is only about 13.9 ml/g at the same pressure. Although their V_L has little difference, the methane adsorption at low pressure differs greatly. This illustrates that the ease of their methane adsorption is different. Coal sample X-2 is easy to adsorb methane, but coal sample X-3 is the opposite. In the process of coalbed gas production, the adsorbing methane of coal sample X-2 is difficult to desorb, but coal sample X-3 is not.

3.2 LP-N_2A isotherms and pore structure characteristics

The characteristic differences of adsorption and desorption isotherms of coal samples represent the development of different types of pores (Yang et al., 2014). For porous media, the LP-N_2A curves may be grouped into six types and hysteresis loops may be divided into four types (Sing, 1985). Figure 3 shows the LP-N_2A isotherms for 11 coal samples. The LP-N_2A isotherms of coals have remarkable differences. Based on the classification scheme proposed by De Boer (De Boer, 1958) and IUPAC (IUPAC, 1982), all coal samples can be classified as three types (A, B, and C) by the characteristics of LP-N_2A isotherms.

Type A is for X-2, X-4, Y-3, Y-4 and Y-6 samples. When $p/p_0 < 0.8$, the adsorption curves increase slowly. The adsorption curves increase rapidly at p/p_0 approaching 1.0. There are inconspicuous hysteresis loops and no inflection points at $0.4 < p/p_0 < 1.0$. But the adsorption and desorption curves nearly overlap at $p/p_0 < 0.4$. The adsorption volume is small at $p/p_0 < 0.4$. At this stage, the pores consist mainly of impermeable pores closed at one end. When $0.4 < p/p_0 < 0.9$,

TABLE 3 Pore characteristics of all the samples based on N_2 adsorption/desorption analysis.

Sample ID	SSA(m^2/g)	PV (cm^3/g)	Average PD (nm)	PV-N_2 (cm^3/g)		SSA-N_2 (m^2/g)		Hysteresis loop types
				<10 nm	>10 nm	<10 nm	>10 nm	
X-1	0.407	0.0027	26.4	0.00045	0.0023	0.236	0.171	B
X-2	1.277	0.0038	12.5	0.0012	0.0026	1.013	0.264	A
X-3	0.989	0.0013	6.6	0.00044	0.00086	0.911	0.078	C
X-4	0.805	0.0035	17.4	0.00082	0.00268	0.577	0.228	A
X-5	0.980	0.0010	3.9	0.00055	0.00045	0.949	0.031	C
Y-1	0.761	0.0035	18.6	0.00053	0.00298	0.514	0.247	B
Y-2	0.657	0.0032	19.5	0.00069	0.00251	0.447	0.210	B
Y-3	0.925	0.0039	16.8	0.00081	0.00309	0.649	0.276	A
Y-4	0.519	0.0017	12.8	0.00048	0.00122	0.399	0.120	A
Y-5	1.037	0.0030	11.6	0.0012	0.00183	0.856	0.181	A
Y-6	0.841	0.0040	18.6	0.00062	0.00338	0.584	0.257	B

TABLE 4 NMR porosity of coal samples.

Sample No.	Irreducible fluid porosity (%)	Moveable fluid porosity (%)	Total porosity (%)
X-1	2.11	1.54	3.65
X-2	5.77	1.48	7.25
X-3	5.02	1.64	6.66
X-4	5.96	1.73	7.69
X-5	4.91	1.24	6.15
Y-1	3.96	1.42	5.38
Y-2	2.89	1.58	4.47
Y-3	4.54	1.02	5.56
Y-4	4.43	1.15	5.58
Y-5	4.62	1.19	5.81
Y-6	4.78	1.51	7.29

the pore was dominated by cylindrical pores with openings at both ends. Due to the obvious adsorption hysteresis loops and the rapid rise of the adsorption curve, the pores are mainly open parallel plate pores at $0.9 < p/p_0 < 1.0$. This shows that the transition pores, mesopores and some micropores of samples have good connectivity. The samples (e.g., X-1, Y-1, Y-2 and Y-6) belong to type B. Their adsorption curves increase steadily at $p/p_0 < 0.8$ and then increase significantly and rapidly at $0.8 < p/p_0 < 1.0$. It is different from type A in that it has a wide hysteresis loop at $0.5 < p/p_0 < 1.0$. When $p/p_0 < 0.4$, most of the pores are impermeable pores closed at one end. But their adsorption and desorption branches have no overlap at $p/p_0 < 0.5$, which is thought to be due to pore swelling and chemical interactions of gas and coal pore surface (Sun et al., 2015; Li et al., 2018). The hysteresis loop indicates that the pores are mainly open cylinder pores at $0.4 < p/p_0 < 0.9$. The desorption curve has an inflection point at a relative pressure of approximately 0.5, which reacts to the presence of thin neck and ink bottle pores. When $0.9 < p/p_0 < 1.0$, the pore types are also open parallel plate pores. Moreover, type C is for X-3 and X-5 samples. The pore types are similar to type B and type C at $p/p_0 < 0.4$, but the hysteresis loop is also not completely closed. When $0.4 < p/p_0 < 0.9$, the appearance of wide hysteresis loops indicates that the pores are mainly composed of open pores, including cylinder pores and wedge pores. The desorption curve has a sharp inflection point at p/p_0 of 0.5, which indicates the presence of a large number of fine bottleneck and ink bottle pores. When $0.9 < p/p_0 < 1.0$, type C differs from other types in having few plate-shaped pores.

The LPN_2GA test results are shown in Table 3. The SSA and PV of coal samples are obviously different. The SSA and

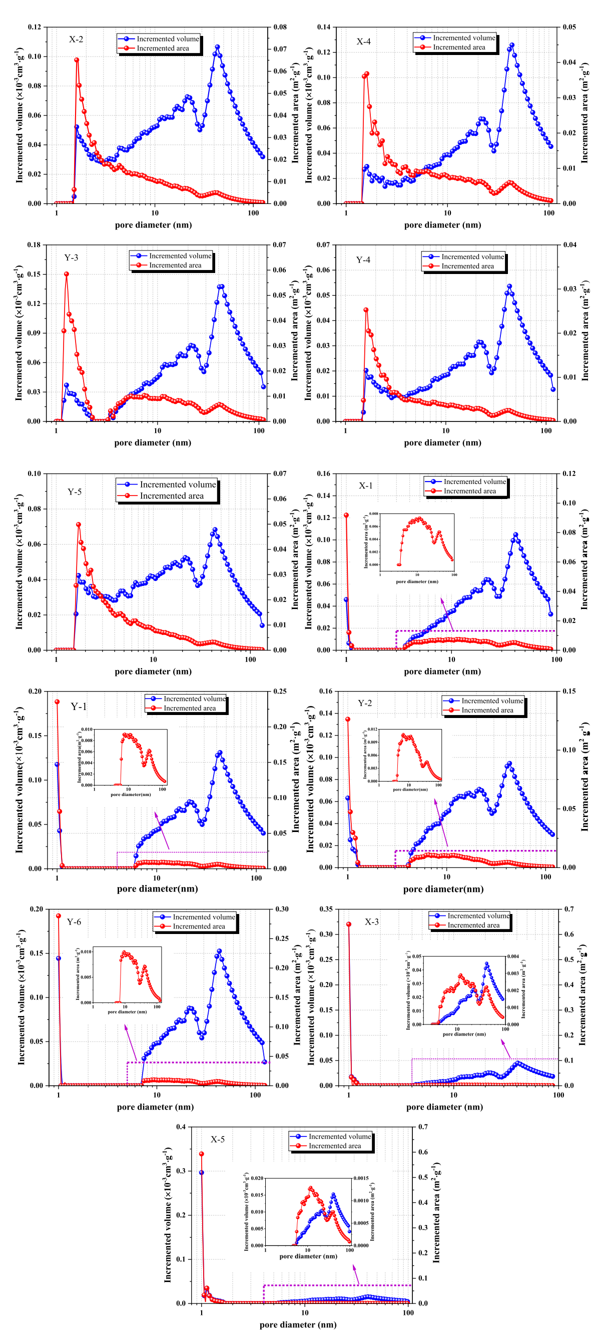

FIGURE 4
The distribution of incremental PV and SSA with LPN_2GA. (X-2, X-4, Y-3, Y-4 and Y-5) Type A, (X-1, Y-1, Y-2 and Y-6) Type B, and (X-3 and X-5) Type C.

PV range from 0.407 to 1.277 m^2/g and 0.001–0.004 cm^3/g, respectively. The PSD of the PV and SSA in different types of coal samples is shown in Figure 4. The SSA distribution curves suggest that all coal samples exhibit unimodality with the main peak at ~1 nm, indicating that the SSA of coal samples is more concentrated in micropores (the SSA for < 10 nm and > 10 nm

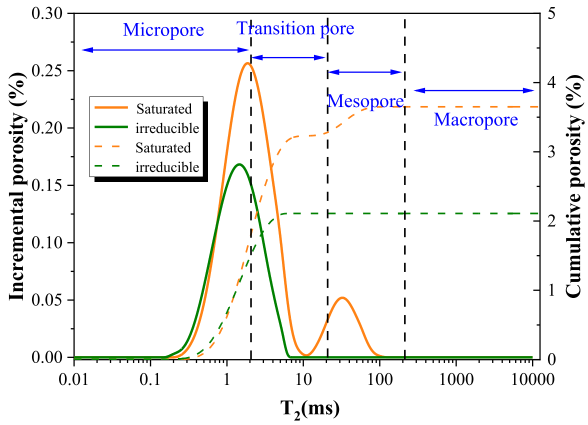

FIGURE 5
NMR T_2 distribution of X-1 coal sample in the saturated water condition and the irreducible water condition.

is 0.236–1.013˚m^2/g and 0.031–0.276˚m^2/g, respectively). Compared with type A, the SSA of type B/C pores is generally undeveloped at > 3 nm. Except for samples X-3 and X-5, the PV distribution shows obvious multimodality in which the peaks of the overall samples are at ~1, ~20 and ~50 nm. The PV for < 10 nm and > 10 nm is 4.4×10-4-1.2×10–3˚cm^3/g and 4.5×10-4-3.38×10–3˚cm^3/g, respectively, indicating that the pores for > 10 nm provide most of the pore volume. Meanwhile, the micropores of type C provide the largest proportion of PV and SSA. Mainly because of the increasing metamorphic degree of coals, the loss of oxygen functional groups and side chains is accompanied by the significant improvement in the degree of aromatization and the increasing and orderly arrangement of aromatic ring layers in the molecular structure of coal, which results in the decrease of larger pores and the increase of smaller pores (Li et al., 2017).

3.3 Pore size distribution of NMR

Previous researches (Cai et al., 2013a; Li et al., 2013) found that T_2 can reflect the PV/size distribution in the saturated water, but cannot provide absolute full-scale PSD. There are two methods to obtain full-scale PSD by NMR measurement, namely centrifugation test and surface relaxation method.

According to the relationship between different centrifugal forces and centrifugal pore radius (Washburn equation), the pore radius r corresponding to the T_2 cutoff value can be obtained at the optimal centrifugal pressure. Yao et al. (2010) propose the centrifugal experiment method of full-

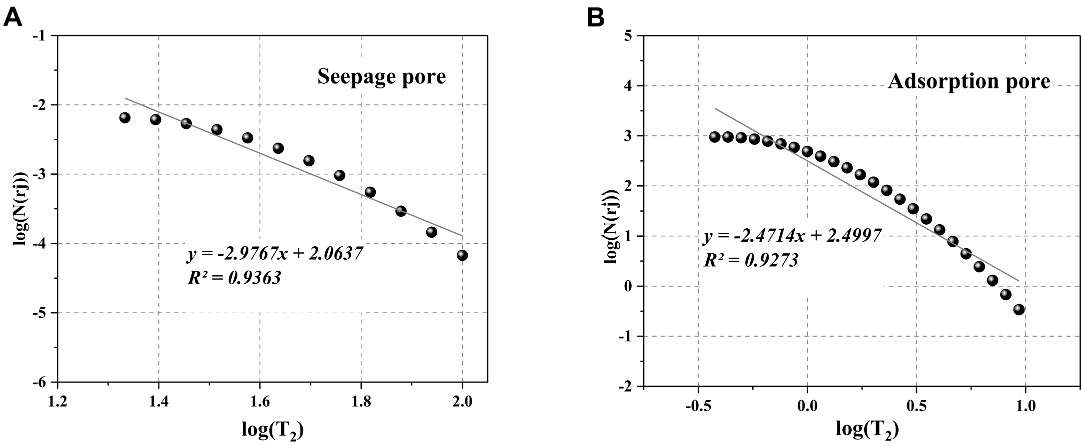

FIGURE 6
The double-logarithm relationship of different pores between log(T_2) vs. log($N(rj)$) for Sample X-1. **(A)** The double-logarithm relationship of seepage pore, **(B)** The double-logarithm relationship of adsorption pore.

TABLE 5 The fractal dimension and correlation coefficient of different pores from NMR data.

Sample No.	D_a	R^2	D_s	R^2
X-1	2.471	0.93	2.976	0.94
X-2	2.805	0.89	2.814	0.91
X-3	2.68	0.91	2.843	0.86
X-4	2.738	0.90	2.819	0.85
X-5	2.612	0.92	-	-
Y-1	2.522	0.98	2.904	0.93
Y-2	2.579	0.92	2.869	0.85
Y-3	2.545	0.88	2.926	0.98
Y-4	2.497	0.88	2.957	0.98
Y-5	2.605	0.91	2.863	0.99
Y-6	2.755	0.89	2.812	0.96

scale PSD of coal reservoir by NMR T_2 cutoff value. The formula can be expressed as

$$r_{ci} = r * T_{2i} / T_{2c} \quad (9)$$

Where r_{ci} (nm) is a pore size corresponding to a relaxation time T_{2i} (ms), T_{2c} is a relaxation time threshold, r (nm) is the pore size corresponding to the T_{2c} and r is about 100 nm.

It is worth noting that there are still some movable fluids in the sample when $T_2 < T_{2C}$. Thus, the centrifugal experiment method is inapplicable. Then, Zheng et al., 2019 proposed a surface relaxation method to calculate the surface relaxivity of different coals, which are 2.1 μm/s, 3.0 μm/s and 1.6 μm/s for low-, medium-, and high-rank coal, respectively.

The pore of coal can be divided into micropores, transition pores, mesopores, and macropores. Micropores and transition pores belong to adsorption pores, mesopores and macropores belong to seepage pores. According to Eq. 2, the T_2 spectrum of coal samples is divided into four parts, corresponding to <2.08 ms, 2.08–20.8 ms, 20.8–208 ms, > 208 ms, and representing different pores: micropore, transition pore, mesopore, macropore, respectively (Figure 5). We also calculated the cumulative porosity in two conditions. The cumulative porosity of other coal samples is given in Table 4. The irreducible and moveable fluid porosity range from 2.11% to 5.96% and 1.02%–1.73%, respectively.

3.4 Characteristics of fractal dimensions in NMR

The fractal dimension of pore structure can be obtained from the slope of the equation by the linear fitting data of log($N(r_j)$) and log(T_2). The linear correlation coefficient for sample X-1 is greater than 0.92, indicating that the adsorption and seepage pore structures of samples can be characterized by the fractal geometry theory (Figure 6). D_a and D_s represent the fractal dimensions of adsorption and seepage pores under the condition of saturated water, respectively. The fractal dimension results of all samples

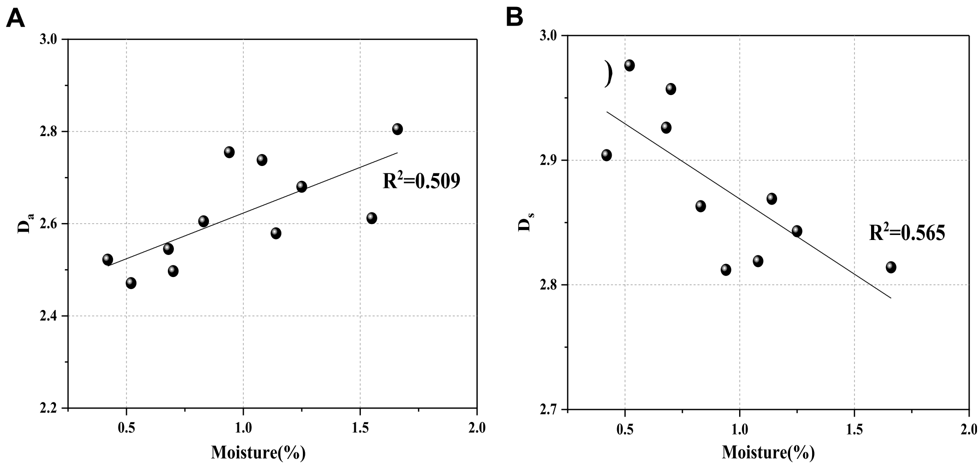

FIGURE 7
Collection between fractal dimensions (D_a and D_s) and moisture content.

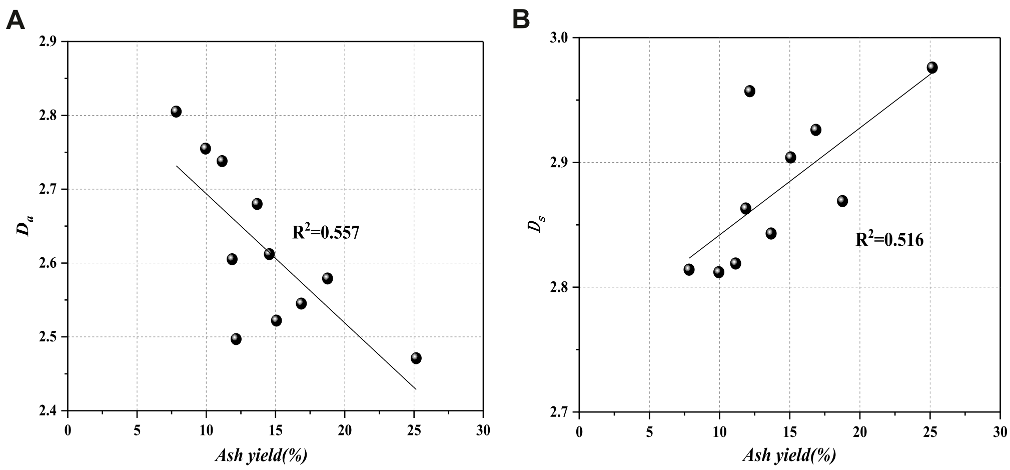

FIGURE 8
Collection between fractal dimensions (D_a and D_s) and ash yield. **(A)** Relationship between D_a and ash yield, **(B)** Relationship between D_s and ash yield.

are listed in Table 5. Generally, the fractal dimension D is between 2 and 3. When fractal dimension D is 2, the pore surface is smooth. When fractal dimension D is 3, the pore surface is rough (Zhang and Weller, 2014). The more complicated rock surface is, the larger D is (Mandelbrot and Benoit, 1998). The ranges of D_a and D_s vary from 2.471 to 2.805 and from 2.812 to 2.976, with the average of 2.619 and 2.878, respectively. Because the relaxation time of the seepage pore is not detected for sample X-5, the fractal dimension of the seepage pore is missing. The fractal dimension D_a is less than D_s, indicating that seepage pores are more complex than adsorption pores in all samples.

4 Discussions

Due to the complex physical properties of coal, the methane adsorption capacity of the coal is affected by many factors, such as coal composition, pore characteristics and so on (Lin et al., 2021). Fractal represents the complexity of coal samples and can be used as a combination of comprehensive factors. However, most previous studies focused on the relationship between the coal permeability and fractal dimension by NMR, so this study mainly discussed the influence of fractal characteristics on methane adsorption capacity for high-rank coals.

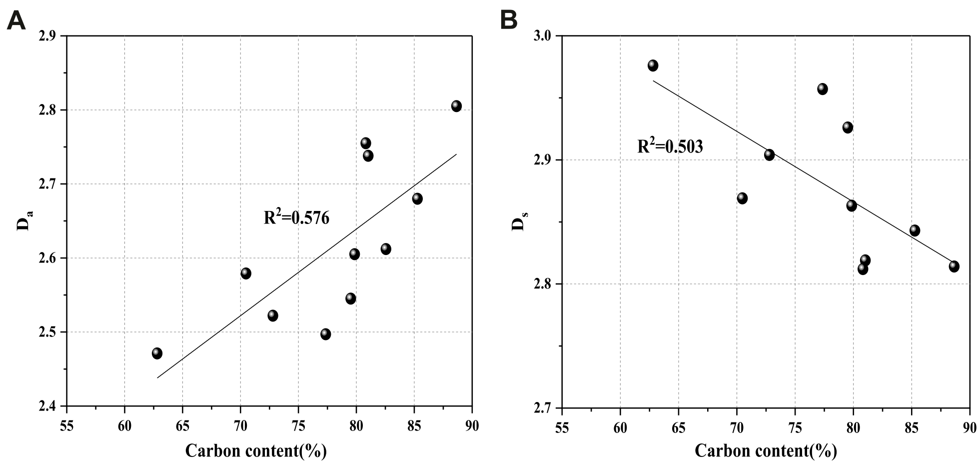

FIGURE 9
Collection between fractal dimensions (D_a and D_s) and carbon content. **(A)** Relationship between D_a and carbon content, **(B)** Relationship between D_s and carbon content.

4.1 Relationships between composition and fractal dimensions of coals

In order to solve the effect of coal composition on fractal characteristics of different coal pore structures by NMR, all correlations between coal compositional parameters and fractal dimensions are shown in Figures 7–9, and the data on coal composition is listed in Table 1.

Figure 7 shows the relationships between moisture contents and fractal dimensions of coals. With the increase of moisture content, fractal dimension D_s decreases (Figure 7B). Yet fractal dimension D_a increases with increasing moisture content (Figure 7A). It means that the fractal dimensions D_a and D_s are greatly influenced by moisture content.

The moisture of coal reservoirs includes free water from seepage pore and irreducible water from adsorption pore. Moisture change in coal is influenced by coal rank. The volume of seepage pore is reduced by compression with the rising of coal rank, but the volume of adsorption pore increases (Yao, et al., 2008). The volume of the adsorption pore increases and that of the seepage pore decreases with the increase of moisture content of high-rank coals, and the surface of the adsorption pore may be influenced by gas-liquid interfacial tension. As a result, the adsorption pore is more complicated, and the seepage pore is more homogeneous (Li et al., 2015).

The relationships between the ash yield and the four fractal dimensions of coals are shown in Figure 8. Ash yield of coals is negatively correlated with D_a (Figure 8A), and positively correlated with D_s (Figure 8B). The mineral content of coal is reflected indirectly by ash yield. If ash yield is high, mineral content is high. With increasing ash yield, adsorption pores may be more homogeneous by filling minerals, which can lead to the decreased fractal dimension D_a. But D_s has a positive correlation with the ash yield of coals. The main reasons are as follows. On the one hand, with increasing ash yield, some seepage pores are partially filled with ash, leading to more heterogeneous structure of seepage pores, and greater fractal dimensions. On the other hand, the newly generated mineral pores lead to enhancing the heterogeneity of seepage pores (Yao et al., 2008; Liu and Wu, 2016).

Figure 9 showsthe relationships between carbon contents and fractal dimensions of coals. With the increase of carbon content, the fractal dimension D_a increases and D_s decreases. We conclude that because of devolatilization and/or oxidation, the high carbon coal usually has low water content and ash yield in the coalification process. In this case, decreasing moisture content and ash yield may have caused the increase of D_a and the decrease of D_s. Meanwhile, the volume and percentage of seepage pores are reducing in coals with increasing carbon contents, which leads to more homogeneous structure of seepage pores.

4.2 Relationships between porosity and fractal dimensions of coals

Figure 10 shows the line relationship between pore structure parameters and fractal dimensions (D_a and D_s). The fractal dimension D_a has a positive linear correlation with the total SSA and SSA of micropore, indicating that

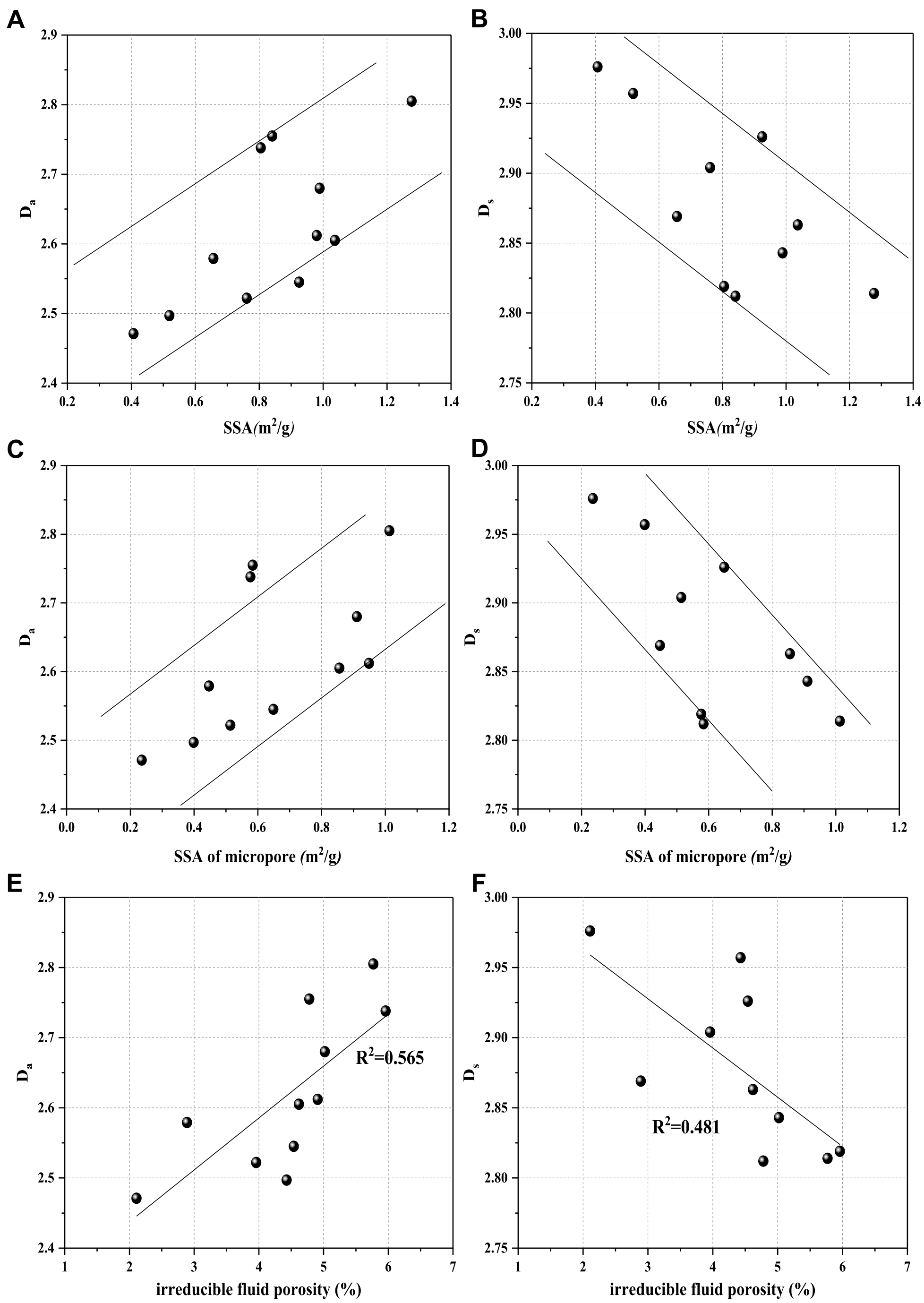

FIGURE 10
Collection between fractal dimension and pore structure. **(A** and **B)** Relationship between fractal dimensions and SSA, **(C** and **D)** Relationship between fractal dimensions and SSA of micropore, **(E** and **F)** Relationship between fractal dimensions and porosity.

high-rank coals with higher total SSA and micropore SSA have higher D_a values (Figure 10A, Figure 10C). This means that the total surface area is mainly provided by micropores for high-rank coals. The higher the total SSA is, the higher the micropore percentage will be, resulting in more complexity of the adsorption pore structure. With the increase of total SSA and micropore SSA, D_s gradually decreases, indicating that the higher the total SSA of high-rank coals is, the smaller the content of seepage pores is, leading to more heterogeneous structure of

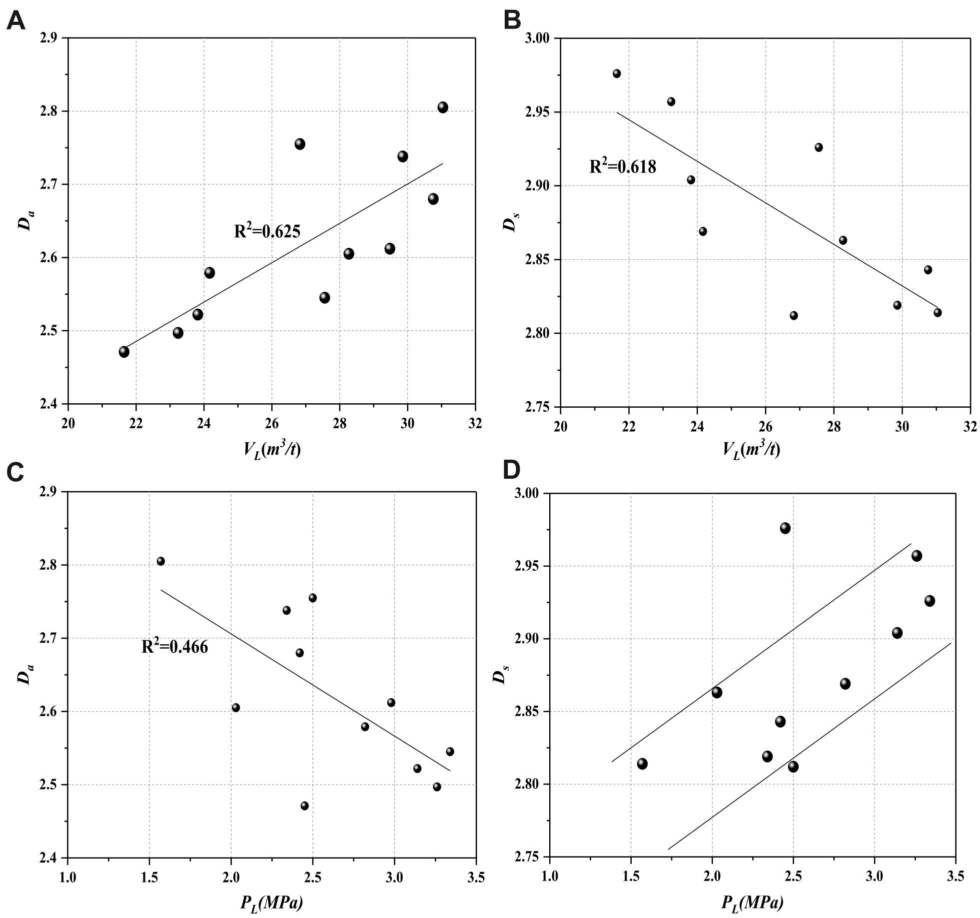

FIGURE 11
Effect of fractal dimensions on methane adsorption. **(A, B)** Relationship between fractal dimensions and V_L, **(B)** Relationship between fractal dimensions and P_L.

seepage pores (Figure 10B, Figure 10D). To further reveal the correlation between fractal dimensions and pore structure characteristics, more information is needed. Table 3 shows the parameters including the total porosity, moveable fluid porosity and irreducible fluid porosity, which are obtained from NMR experimental analysis. The D_a has a positive correlation with the irreducible fluid porosity (Figure 10E). In contrast, The fractal dimensions D_s has a negative correlation with the irreducible fluid porosity (Figure 10F). This means that with increasing irreducible fluid porosity, the volume and percentage of adsorption pores are increasing, which leads to the increase of SSA, more complicated structure of adsorption pores and more heterogeneous structure of seepage pores for high-rank coals. Therefore, they may result in relatively high CH_4 adsorption capacity of coals with higher D_a and less D_s value.

4.3 Relationship between coal adsorption capacity and fractal dimension

The influence of fractal dimensions of different coal samples on V_L and P_L is shown in Figure 11. As shown in Figure 11A and Figure 11B, V_L gradually increases with the increase of D_a, which illustrates that the ultimate adsorption capacity of coal samples is gradually enhanced. V_L has a positive linear correlation with D_a. However, V_L has a negative correlation with D_s, which means that the increase of the D_s value results in a decrease in CH_4 adsorption capacity. The analysis shows that D_a and D_s reflect the fractal feature of adsorption and seepage pores, respectively. As is well-known, the adsorption pore has the primary influence on the adsorption capacity of coal. On the one hand, the higher D_a value represents more SSA of high-rank coals which provide more adsorption sites for CH_4, so the high-rank coals have stronger adsorption capacity with higher D_a. On the other hand, with the increase of D_s value, the high-rank coals have stronger heterogeneity of seepage pore structure, fewer adsorption sites for CH_4 and higher capillary condensation on pore surfaces, which leads to the reduction of CH_4 adsorption. Above all, the fractal dimension D_a affects on CH_4 adsorption capacity greater than D_s.

In the Langmuir equation, P_L, which reflects the adsorption capacity of coal at the low-pressure stage, represents the adsorption pressure when the adsorption volume of CH_4 gets to half of V_L. The influence of the fractal dimensions D_a and D_s on P_L is shown in Figure 11C and Figure 11D. As can be seen from the figures, The D_a value is negatively correlated with P_L. The CH_4 adsorption velocity of coal samples is increasing. According to the volume filling theory of micropores (Carrott et al., 1987), the micropores with the adsorption potential of significant superposition can reach saturation of adsorption capacity at lower pressure, and the adsorption energy has a close relationship with the surface of the micropores. With the increase of D_a value, the percentage and surface of micropores will increase, which causes the increase of CH_4 adsorption velocity for high-rank coals. However, there is a positive correlation between P_L and D_s. With the increase of D_s, the percentage of seepage pores will increase and the surface of micropores will decrease. So the CH_4 adsorption velocity decreases with higher D_s value for high-rank coals. Therefore, the fractal dimension D_a has an important influence on P_L.

Since the physical properties of coal are complicated, the difference in fractal dimensions of coal samples is caused by multiple factors, such as the content of each component in coal, pore size distribution, and so on. The above factors result in the heterogeneity of coal surface and structure, which will influence the methane adsorption capacity of coal. Thus, the fractal dimensions are the comprehensive reflection of differences among the physical properties of coal and are able to show the effect of coal properties on methane adsorption fully.

5 Conclusion

1. According to the characteristics of LP-N_2A isotherms, all coal samples can be classified into three types. The SSA distribution curves exhibit unimodality with the main peak at ~1 nm for all coal samples, indicating that the SSA of high-rank coals is more concentrated in micropores. The PV distribution shows obvious multimodality for most coal samples, and the peaks are at ~1, ~20 and ~50 nm. The pores for > 10 nm provide most of the pore volume. Meanwhile, the micropores of type C provide the largest proportion of PV and SSA.
2. We divide the T_2 spectrum of coal samples into four parts by the surface relaxivity of high-rank coal. Meanwhile, the fractal dimensions of different pore types are obtained from the slope of the equation by the linear fitting data of $\log(N(r_j))$ and $\log(T_2)$. The average values of D_a and D_s are 2.619 and 2.878, respectively.
3. The composition and pore parameters of coals have much greater control over fractal dimensions. The fractal dimension D_a has a negative correlation with ash yield and moisture content, and a positive correlation with carbon content. The fractal dimension D_s has a positive correlation with ash yield and moisture content, and a negative correlation with carbon content. The high-rank coals with higher D_a value have the more complicated structure of adsorption pores with higher SSA and irreducible fluid porosity, which results in relatively high CH_4 adsorption capacity of coals.
4. The different fractal dimensions have varying effects on methane adsorption. With the increase of fractal dimension D_a, V_L increased and P_L decreased, which illustrates that the CH_4 adsorption capacity and velocity are gradually enhanced for high-rank coals. Compared with Da, Ds has the opposite effect on the CH_4 adsorption capacity and velocity of high-rank coals. Thus, the fractal dimensions of different pore types, which are calculated based on NMR, are able to show the effect of coal properties on CH_4 adsorption fully.

Data availability statement

The original contributions presented in the study are included in the article/Supplementary Material, further inquiries can be directed to the corresponding author.

Author contributions

WJ: laboratory experiments and data analysis; YZ: manuscript preparation; CW: manuscript review; and MD: sample collection.

Funding

This study was financially supported by the start-up fund for doctoral research of Suzhou University (No.2019jb16), Scientific research platform project of Suzhou University (2021XJPT54) and College Students' innovation and entrepreneurship training program of Suzhou University (KYLXYBXM22-070).

Conflict of interest

The authors declare that the research was conducted in the absence of any commercial or financial relationships that could be construed as a potential conflict of interest.

Publisher's note

All claims expressed in this article are solely those of the authors and do not necessarily represent those of their affiliated organizations, or those of the publisher, the editors and the reviewers. Any product that may be evaluated in this article, or claim that may be made by its manufacturer, is not guaranteed or endorsed by the publisher.

References

Acevedo, B., and Barriocanal, C. (2015). Texture and surface chemistry of activated carbons obtained from tyre wastes. *Fuel Process. Technol.* 134, 275–283. doi:10.1016/j.fuproc.2015.02.009

Alexeev, A. D., Vasilenko, T., and Ulyanova, E. (1977). Closed porosity in fossil coals. *Fuel* 78, 635–638. doi:10.1016/s0016-2361(98)00198-7

Barrett, E. P., Joyner, L. G., and Halenda, P. P. (1951). The determination of pore volume and area distributions in porous substances. I. computations from nitrogen isotherms. *J. Am. Chem. Soc.* 73, 373–380. doi:10.1021/ja01145a126

Brunauer, S., Emmett, S., and Teller, E. J. (1938). Adsorption of gases in multi-molecular layers. *J. Am. Chem. Soc.* 60 (2), 309–319. doi:10.1021/ja01269a023

Cai, Y., Liu, D., Pan, Z., Yao, Y., Li, J., and Qiu, Y. (2013b). Pore structure and its impact on CH_4 adsorption capacity and flow capability of bituminous and subbituminous coals from northeast China. *Fuel* 103, 258–268. doi:10.1016/j.fuel.2012.06.055

Cai, Y., Liu, D., Pan, Z., Yao, Y., and Qiu, Y. (2013a). Petrophysical characterization of Chinese coal cores with heat treatment by nuclear magnetic resonance. *Fuel* 108 (11), 292–302. doi:10.1016/j.fuel.2013.02.031

Carrott, P., Roberts, R. A., and Sing, K. (1987). Adsorption of nitrogen by porous and non-porous carbons. *Carbon* 25 (1), 59–68. doi:10.1016/0008-6223(87)90040-6

Chen, Y., Liu, D., and Gan, Q. (2018). Insights into fractal characteristics of pores in different rank coals by nuclear magnetic resonance (NMR). *Arab. J. Geosci.* 11 (19), 578. doi:10.1007/s12517-018-3943-2

Cheng, Y. Y., Cheng, Z. L., Li, S., Chen, S. D., and Guo, T. (2021). Characteristics of coalbed methane accumulation in Bide-Santang syncline, Western Guizhou and favorable sector. *Geol. Bull. China* 40 (7), 1140–1148.

Coetzee, G. H., Sakurovs, R., Neomagus, W., Hein, J. P., Everson, R. C., Mathews, J. P., et al. (2015). Pore development during gasification of South African inertinite-rich chars evaluated using small angle X-ray scattering. *Carbon* 95, 250–260. doi:10.1016/j.carbon.2015.08.030

Daigle, H., and Johnson, A. (2016). Combining mercury intrusion and nuclear magnetic resonance measurements using percolation theory. *Transp. Porous Media* 111, 669–679. doi:10.1007/s11242-015-0619-1

De Boer, J. H. (1958). *The shape of capillaries*. Landon: Butterworth.

Dillinger, A., and Esteban, L. (2014). Experimental evaluation of reservoir quality in Mesozoic formations of the Perth Basin (Western Australia) by using a laboratory low field nuclear magnetic resonance. *Mar. Petroleum Geol.* 57, 455–469. doi:10.1016/j.marpetgeo.2014.06.010

Dullien, F. A. L. (1991). *Porous media fluid transport and pore structure*. Massachusetts, United States: Academic Press.

Ferro, N. D., Delmas, P., Duwig, C., Simonetti, G., and Morari, F. (2012). Coupling X-ray microtomography and mercury intrusion porosimetry to quantify aggregate structures of a cambisol under different fertilisation treatments. *Soil Tillage Res.* 119, 13–21. doi:10.1016/j.still.2011.12.001

Fu, X. H., Qin, Y., Zhang, W. H., Wei, C. T., and Zhou, R. F. (2005). Fractal classification and natural classification of coal pore structure based on migration of coalbed methane. *Chin. Sci. Bull.* 50, 66–71. doi:10.1007/bf03184085

Gao, Sh., Wang, L., Gao, J., and Zhang, R. (2018). Experimental study on pore structures of hard coal with different metamorphic grade based on fractal theory. *Coal Sci. Tech.* 46 (8), 93–100. doi:10.13199/j.cnki.cst.2018.08.015

Ge, X., Fan, Y., Zhu, X., Chen, Y., and Li, R. (2014). Determination of nuclear magnetic resonance T_2 cutoff value based on multifractal theory-An application in sandstone with complex pore structure. *Geophysics* 80 (1), 11–21. doi:10.1190/geo2014-0140.1

Geerlings, P., Proft, F. D., and Langenaeker, W. (2003). Conceptual density functional theory. *Chem. Rev.* 103 (29), 1793–1874. doi:10.1021/cr990029p

Hodot, B. B. (1966). *Outburst of coal and coalbed gas*. Beijing: China Industry Press.

IUPAC (1982). Reporting physisorption data for gas/solid systems with special reference to the determination of surface area and porosity. *Pure Appl. Chem.* 54 (11), 2201–2218. doi:10.1351/pac198557040603

Johnson, R. C., and Flores, R. M. (1998). Developmental geology of coalbed methane from shallow to deep in Rocky Mountain basins and in Cook inlet Matanuska basin, Alaska, USA and Canada. *Int. J. Coal Geol.* 35 (1), 241–282. doi:10.1016/s0166-5162(97)00016-5

Ju, Y., Sun, Y., Tan, J., Bu, H., Han, K., Li, X., et al. (2018). The composition, pore structure characterization and deformation mechanism of coal-bearing shales from tectonically altered Coalfields in Eastern China. *Fuel* 234, 626–642. doi:10.1016/j.fuel.2018.06.116

Lai, J., Wang, G., Fan, Z., Zhou, Z., Chen, J., and Wang, S. (2018). Fractal analysis of tight shaly sandstones using nuclear magnetic resonance measurements. *Am. Assoc. Pet. Geol. Bull.* 102 (2), 175–193. doi:10.1306/0425171609817007

Lee, B. H., and Lee, S. K. (2013). Effects of specific surface area and porosity on cube counting fractal dimension, lacunarity, configurational entropy, and permeability of model porous networks: Random packing simulations and NMR micro-imaging study. *J. Hydrology* 496, 122–141. doi:10.1016/j.jhydrol.2013.05.014

Li, P., L., Zhang, X., and Zhang, S. (2018). Structures and fractal characteristics of pores in low volatile bituminous deformed coals by low-temperature N_2 adsorption after different solvents treatments. *Fuel* 224, 661–675. doi:10.1016/j.fuel.2018.03.067

Li, X., Kang, Y., and Haghighi, M. (2017). Investigation of pore size distributions of coals with different structures by nuclear magnetic resonance (NMR) and mercury intrusion porosimetry (MIP). *Measurement* 116, 122–128. doi:10.1016/j.measurement.2017.10.059

Li, Y., Yang, J., Pan, Z., and Tong, W. (2020a). Nanoscale pore structure and mechanical property analysis of coal: An insight combining AFM and SEM images. *Fuel* 260, 116352. doi:10.1016/j.fuel.2019.116352

Li, Z., Hao, Z., Pang, Y., and Gao, Y. (2015). Fractal dimensions of coal and their influence on methane adsorption. *J. China Coal Soc.* 40 (4), 863–869. doi:10.13225/j.cnki.jccs.2014.3022

Li, Z., Liu, D., Cai, Y., and Si, G. (2020b). Evaluation of coal petrophysics incorporating fractal characteristics by mercury intrusion porosimetry and low-field NMR. *Fuel (Lond).* 263, 116802. doi:10.1016/j.fuel.2019.116802

Li, Z., Liu, D., Cai, Y., and Teng, J. (2019). Adsorption pore structure and its fractal characteristics of coals by N_2 adsorption/desorption and FESEM image analyses. *Fuel* 257, 116031. doi:10.1016/j.fuel.2019.116031

Li, Z. W., Lin, B. Q., Hao, Z. Y., and Gao, Y. B. (2013). Characteristics of pore size distribution of coal and its impacts on gas adsorption. *J. China Univ. Min. Technol.* 42 (6), 1047–1053. doi:10.13247/j.cnki.jcumt.2013.06.025

Lin, Y., Qin, Y., and Duan, Z. (2021). Pore structure, adsorptivity and influencing factors of high-volatile bituminous coal rich in inertinite. *Fuel* 293, 120418. doi:10.1016/j.fuel.2021.120418

Liu, H. H., Sang, S. X., Liu, S. Q., and Zhu, Q. P. (2015). Growth characteristics and genetic types of pores and fractures in a high-rank coal reservoir of the southern Qinshui basin. *Ore Geol. Rev.* 64, 140–151. doi:10.1016/j.oregeorev.2014.06.018

Liu, S., and Wu, C. (2016). Study on fractal characteristics of different scales pore coal reservoir in Bide-Santang Basin. *Coal Sci. Technol.* 44 (2), 33–38. doi:10.13199/j.cnki.cst.2016.02.006

Liu, X. F., and He, X. Q. (2017). Effect of pore characteristics on coalbed methane adsorption in middle-high rank coals. *Adsorption* 23 (1), 3–12. doi:10.1007/s10450-016-9811-z

Mandelbrot, B. B., and Benoit, B. (1998). The fractal geometry of nature. *Am. J. Phys.* 51 (3), 286–287. doi:10.1119/1.13295

Meyers, R. A. (1982). *Coal structure*. New York: Academic Press.

Nie, B., Lun, J., Wang, K., and Shen, J. (2020). Three-dimensional characterization of open and closed coal nanopores based on a multi-scale analysis including CO2 adsorption, mercury intrusion, low-temperature nitrogen adsorption, and small-angle X-ray scattering. *Energy Sci. Eng.* 8, 2086–2099. doi:10.1002/ese3.649

Ouyang, Z., Liu, D., Cai, Y., and Yao, Y. (2016). Fractal analysis on heterogeneity of pore-fractures in middle-high rank coals with NMR. *Energy fuels.* 30, 5449–5458. doi:10.1021/acs.energyfuels.6b00563

Pan, J., Zhu, H., Hou, Q., Wang, H., and Wang, S. (2015). Macromolecular and pore structures of Chinese tectonically deformed coal studied by atomic force microscopy. *Fuel* 139, 94–101. doi:10.1016/j.fuel.2014.08.039

Peng, C., Zou, C., Yang, Y., Zhang, G., and Wang, W. (2017). Fractal analysis of high rank coal from southeast Qinshui basin by using gas adsorption and mercury porosimetry. *J. Petroleum Sci. Eng.* 156, 235–249. doi:10.1016/j.petrol.2017.06.001

Saboorian-Jooybari, H. (2016). New analytical formulas for prediction of gas-liquid relative permeabilities through fractures-Part I: Incompressible flow. *J. Nat. Gas Sci. Eng.* 30, 604–615. doi:10.1016/j.jngse.2016.02.002

Shan, C., Zhang, T., Guo, J., Zhang, Z., and Yang, Y. (2015). Characterization of the micropore systems in the high-rank coal reservoirs of the southern Sichuan Basin, China. *Am. Assoc. Pet. Geol. Bull.* 99 (11), 2099–2119. doi:10.1306/07061514240

Shi, Y. M., Zhang, Y. G., Yong, H. E., Zheng, H. F., Lu, W. Z., and Zheng, H. J. (2006). The study of flow units using fractal and fractal dimension methods of capillary pressure curve. *Earth Sci. Front.* 13 (3), 129–134.

Sing, K. S. W. (1982). Reporting physisorption data for gas/solid systems with special reference to the determination of surface area and porosity (Provisional). *Pure Appl. Chem.* 54 (11), 2201–2218. doi:10.1351/pac198254112201

Sing, K. S. W. (1985). Reporting physisorption data for gas/solid systems with special reference to the determination of surface area and porosity (Recommendations 1984). *Pure Appl. Chem.* 57, 603–619. doi:10.1351/pac198557040603

Song, X. X., Tang, Y. G., Wei, L. I., Wang, S. Q., and Yang, M. X. (2013). Fractral characteristics of adsorption pores of tectonic coal from Zhongliangshan southern coalmine. *J. China Coal Soc.* 38 (1), 134–139. doi:10.13225/j.cnki.jccs.2013.01.002

Song, Y., Jiang, B., and Liu, J. (2017). Nanopore structural characteristics and their impact on methane adsorption and diffusion in low to medium tectonically deformed coals: Case study in the huaibei coal field. *Energy fuels.* 31 (7), 6711–6723. doi:10.1021/acs.energyfuels.7b00512

Sun, W., Feng, Y., Jiang, C., and Chu, W. (2015). Fractal characterization and methane adsorption features of coal particles taken from shallow and deep coalmine layers. *Fuel* 155, 7–13. doi:10.1016/j.fuel.2015.03.083

Wang, C., Jiang, C. F., and Wei, C. (2013). Fractral dimension of coals and analysis of its influencing factors. *J. China Univ. Min. Technol.* 42 (6), 1009–1014. doi:10.13247/j.cnki.jcumt.2013.06.020

Wang, L. G., Jesus, M., and Salazar, J. (2011). Effects of surfactant-emulsified oil-based mud on borehole resistivity measurements. *SPE J.* 16 (3), 608–624. doi:10.2118/109946-pa

Yang, Z., Qin, Y., Wang, G. X., and An, H. (2014). Investigation on coal seam gas formation of multi-coalbed reservoir in Bide-Santang Basin Southwest China. *Arab. J. Geosci.* 8, 5439–5448. doi:10.1007/s12517-014-1640-3

Yang, Z., Qin, Y., Yi, T., Tang, J., Zhang, Z., and Wu, C. (2019). Analysis of multi-coalbed CBM development methods in Western Guizhou, China. *Geosci. J.* 23, 315–325. doi:10.1007/s12303-018-0037-9

Yao, Y., and Liu, D. (2012). Comparison of low-field NMR and mercury intrusion porosimetry in characterizing pore size distributions of coals. *Fuel* 95 (1), 152–158. doi:10.1016/j.fuel.2011.12.039

Yao, Y., Liu, D., Tang, D., Tang, S., and Huang, W. (2008). Fractal characterization of adsorption-pores of coals from North China: An investigation on CH_4 adsorption capacity of coals. *Int. J. Coal Geol.* 73, 27–42. doi:10.1016/j.coal.2007.07.003

Yao, Y., Liu, D., Tang, D., Tang, S., Huang, W., Liu, Z., et al. (2009). Fractal characterization of seepage-pores of coals from China: An investigation on permeability of coals. *Comput. Geosci.* 35 (6), 1159–1166. doi:10.1016/j.cageo.2008.09.005

Yao, Y., Liu, D., Yao, C., Tang, D., Tang, S., and Huang, W. (2010). Petrophysical characterization of coals by low-field nuclear magnetic resonance (NMR). *Fuel* 89 (7), 1371–1380. doi:10.1016/j.fuel.2009.11.005

Zhang, C., Chen, Z., and Zhang, Z. (2007). Fractal characteristics of reservoir rock pore structure based on NMR T_2 distribution. *J. Oil Gas Technol.* 29 (4), 80–86.

Zhang, Z., and Weller, A. (2014). Fractal dimension of pore-space geometry of an Eocene sandstone formation. *Geophysics* 79 (6), 377–387. doi:10.1190/geo2014-0143.1

Zhao, D., Guo, Y., Wang, G., and Mao, X. (2019). Characterizing nanoscale pores and its structure in coal: Experimental investigation. *Energy Explor. Exploitation* 37 (4), 1320–1347. doi:10.1177/0144598719831397

Zheng, S., Yao, Y., Elsworth, D., and Liu, Y. (2020). A novel pore size classification method of coals: Investigation based on NMR relaxation. *J. Nat. Gas Sci. Eng.* 81, 103466. doi:10.1016/j.jngse.2020.103466

Zheng, S., Yao, Y., Liu, D., Cai, Y., Liu, Y., and Li, X. (2019). Nuclear magnetic resonance T_2 cutoffs of coals: A novel method by multifractal analysis theory. *Fuel* 241, 715–724. doi:10.1016/j.fuel.2018.12.044

Zhou, S., Liu, D., Cai, Y., and Yao, Y. (2016). Fractal characterization of pore–fracture in low-rank coals using a low-field NMR relaxation method. *Fuel* 181, 218–226. doi:10.1016/j.fuel.2016.04.119

Zhou, S., Liu, D., Karpyn, T., and Yao, Y. (2018). Effect of coalification jumps on petrophysical properties of various metamorphic coals from different coalfields in China. *J. Nat. Gas Sci. Eng.* 60, 63–76. doi:10.1016/j.jngse.2018.10.004

Zhou, S., Wang, H., Jiang, S., Yan, D., Guoqing, L., Zhang, Z., et al. (2022). A novel approach to obtain fractal dimension in coals by LFNMR: Insights from the T_2 peak and T_2 geometric mean. *J. Energy Eng.* 148 (3), 0000827. doi:10.1061/(asce)ey.1943-7897.0000827